Magnetic field-temperature phase diagrams of multiferroic $(Ni_{0.9}Co_{0.1})_3V_2O_8$

N. Qureshi,[1,*] E. Ressouche,[2] A. A. Mukhin,[3] V. Yu. Ivanov,[3] S. N. Barilo,[4] S. V. Shiryaev,[4] and V. Skumryev[5]

[1]*Institut Laue-Langevin, 71 avenue des Martyrs, CS 20156, 38042 Grenoble Cedex 9, France*

[2]*SPSMS, UMR-E CEA/UJF-Grenoble 1, INAC, 38054 Grenoble, France*

[3]*Prokhorov General Physics Institute, Russian Academy of Sciences, ulica Vavilova 38, Moscow, 119991 Russia*

[4]*Institute of Solid State and Semiconductor Physics, National Academy of Sciences of Belarus, Minsk 220072, Belarus*

[5]*Institució Catalana de Recerca i Estudis Avançats and Departament de Física, Universitat Autónoma de Barcelona, 08193 Bellaterra, Spain*

(Received 13 June 2016; revised manuscript received 10 October 2016; published 28 November 2016)

We present macroscopic and neutron diffraction data on multiferroic lightly Co doped $Ni_3V_2O_8$. The magnetic H-T phase diagrams have been derived from magnetization and electric polarization measurements with field directions parallel to the principal crystallographic axes. While the phase diagram for $H \parallel b$ is very similar to that of the parent compound $Ni_3V_2O_8$ for the commonly involved phases, the zero-field phases in $(Ni_{0.9}Co_{0.1})_3V_2O_8$ show a stronger instability for applied magnetic fields along the a or c axis. Neutron single-crystal diffraction revealed the magnetic structure of the field-induced phase for $H \parallel c$ with a collinear spin alignment along the a and b axes for the two magnetically inequivalent sites. A pronounced irreversibility has been observed for the transition between the zero-field spin cycloid and the field-induced phase, which is manifested in a propagation vector change from $\mathbf{q} = (0.322\ 0\ 0)$ to $\mathbf{q} = (0.306\ 0\ 0)$, with slight modifications of the magnetic structure after reentering the zero-field phase. The reentrant phase is characterized by a significantly larger b component of the cross-tie site spin, therefore showing remanent features of the high-field phase. For $H \parallel a$ the magnetization data reveal anomalies, one of which was proved to reflect a field-induced transition from the cycloidally to the sinusoidally modulated magnetic structure.

DOI: 10.1103/PhysRevB.94.174441

I. INTRODUCTION

Multiferroic materials [materials combining at least two of the ferroic states, e.g., (anti)ferromagnetism and ferroelectricity] have drawn significant scientific interest due to their promising role in future applications (for an extensive review of multiferroics and magnetoelectrics the reader is referred to Refs. [1–5]). Depending on the origin of the ferroelectric polarization multiferroic materials are classified into two groups: proper (type-I) and improper (type-II) multiferroics. In the latter, the electric polarization appears as a by-product of the magnetic ordering, and therefore, the two phenomena are intimately coupled. This ability to control the magnetic properties by an electric field and vice versa, the so-called magnetoelectric effect, renders these compounds highly interesting for use as data storage devices. Although the absolute value of the ferroelectric polarization in improper multiferroics is rather low, the magnetoelectric effect is very strong in comparison to the proper ones. However, multiferroics, in which the electric polarization is induced by a complex magnetic order originating from competing exchange interactions, usually have rather low magnetic ordering temperatures, well below 100 K (except for CuO with an onset of ferroelectricity at 230 K [6,7]), which still does not allow exploitation of this phenomenon for device application. Engineered magnetoelectric heterostructures using thin films of sandwiched magnetostrictive and piezoelectric materials have also triggered huge research activity. An intensively studied improper multiferroic compound is the kagome staircase system $Ni_3V_2O_8$ crystallizing in the orthorhombic space group $Cmce$ [8,9] and revealing a sequence of four magnetic phase transitions [10–14]. Like for other multiferroic compounds, first, a sinusoidally modulated incommensurate phase is entered upon lowering the temperature, which is then followed by an incommensurate spiral magnetic structure breaking inversion symmetry and therefore inducing a net ferroelectric polarization via the Dzyaloshinskii-Moriya interaction. Upon further reduction of the temperature the single-ion anisotropy term dominates the Hamiltonian for which the ground states are simple commensurate antiferromagnets. Interestingly, doping a low amount of Co into this system lowers the magnetic phase-transition temperatures and suppresses the low-temperature commensurate phases at least above 1.8 K [15–20]. A comparison of the transition temperatures in undoped $Ni_3V_2O_8$ ($x = 0$), $(Ni_{0.93}Co_{0.07})_3V_2O_8$ ($x = 0.07$), and $(Ni_{0.9}Co_{0.1})_3V_2O_8$ ($x = 0.1$) is shown in Fig. 1. Higher doping levels of Co also change the types of magnetic structures, as has been shown by macroscopic measurements and neutron diffraction [21–23]. Here we present macroscopic and neutron diffraction measurements on multiferroic $(Ni_{0.9}Co_{0.1})_3V_2O_8$, revealing the magnetic phase diagrams as a function of temperature and the applied magnetic field along the crystallographic axes. Preliminary magnetic studies on this compound in fields up to 5 T were reported in Ref. [17].

II. EXPERIMENT

All measurements were performed on the same single-crystal samples as used in Ref. [20]. The magnetization was measured as a function of temperature and magnetic field using a superconducting quantum interference device (SQUID) magnetometer and a Physical Property Measurement System from Quantum Design. The ac susceptibility was measured at 10 Oe and 100 Hz, also in a superimposed dc field (i.e., the so-called incremental susceptibility). The magnetic

*Corresponding author: qureshi@ill.fr

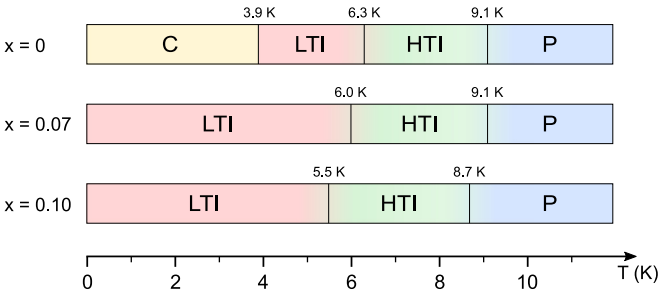

FIG. 1. Magnetic phase transitions in $(Ni_{1-x}Co_x)_3V_2O_8$ for $x = 0$, 0.07, and 0.10. The transition temperatures were taken from Refs. [11,20].

field was applied within a few degrees of accuracy along the principal crystallographic directions of the crystals (shaped as a $3 \times 2 \times 5\,mm^3$ parallelepiped along the crystallographic a, b, and c axes, respectively). The data presented here are not corrected for the demagnetizing field effect. The electric polarization was studied along the b axis (coinciding with the shortest dimension of a 0.75-mm plateletlike sample with an area of 4 mm^2) by pyroelectric measurements using a Keithley 6517A electrometer. A poling electric field $E \sim 1.3$ kV/cm was applied while cooling down the sample through the Néel temperature in order to obtain a single polar domain state for which the field was continuously applied during the magnetic-field or temperature-dependent polarization experiments. The neutron diffraction experiments were carried out at the four-circle diffractometers D23 and D10 (ILL, Grenoble) using wavelengths of 1.28 and 1.26 Å, respectively, from a Cu(200) monochromator. The nuclear and magnetic structures have been investigated according to the temperature- and field-induced magnetic phase transitions seen by the macroscopic methods. All integrated intensities were corrected for absorption by applying the transmission factor integral $\exp[-\mu(\tau_{in} + \tau_{out})]$ using subroutines of the Cambridge Crystallographic Subroutine Library [24] [τ_{in} and τ_{out} represent the path lengths of the beam inside the crystal before and after the diffraction process, and μ is the linear absorption coefficient, which is 0.145 cm^{-1} for $(Ni_{0.9}Co_{0.1})_3V_2O_8$].

III. RESULTS AND DISCUSSION

A. Macroscopic measurements

The real part of the magnetic susceptibility has been investigated as a function of temperature and magnetic field for applied field directions along the main crystallographic axes. Figure 2 shows the temperature dependence with the zero-field magnetic phase-transition temperatures marked with dashed lines as a reference [20]. At the Néel temperature the system undergoes a magnetic phase transition into the high-temperature incommensurate (HTI) phase in which the magnetic moments are sinusoidally modulated. It can be seen that this phase transition is shifted towards lower temperatures upon applying a magnetic field along either of the main crystallographic axes. At low magnetic fields a second magnetic phase transition into the low-temperature incommensurate (LTI) phase, a cycloidal magnetic structure inducing a net

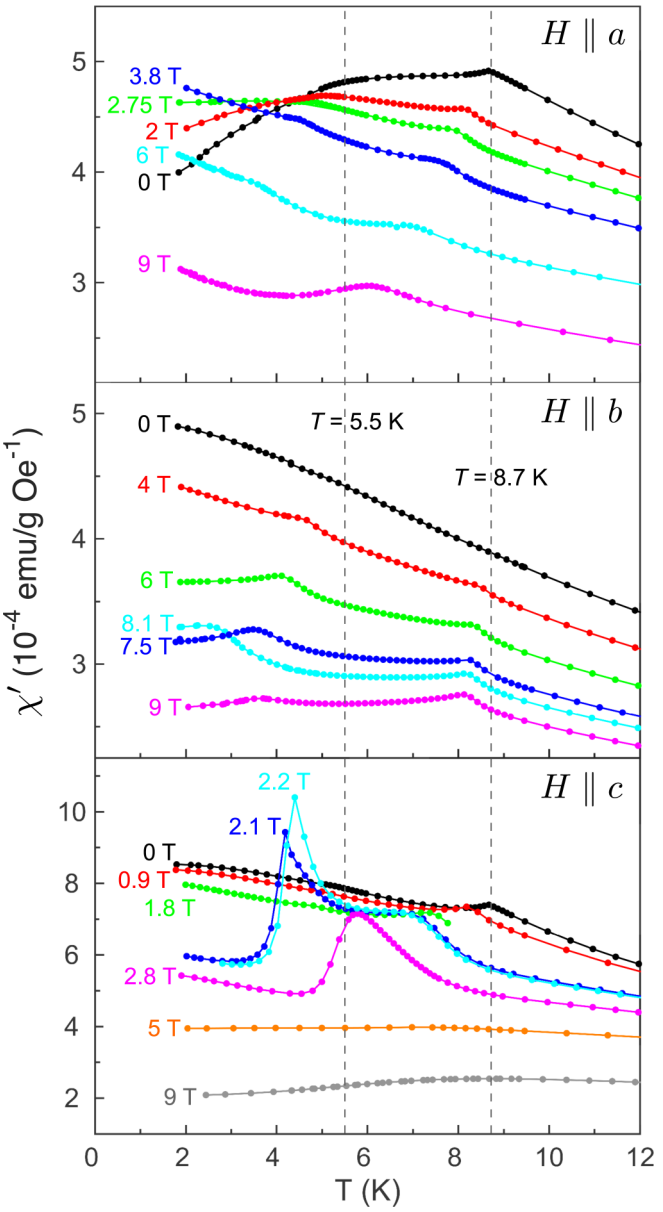

FIG. 2. Real part of the ac magnetic susceptibility as a function of temperature for superimposed dc magnetic fields applied along the a (top panel), b (middle panel), and c axes (bottom panel). All data shown were recorded on warming up after a zero-field-cooling procedure.

electric polarization, takes place (note that we use the same nomenclature for the magnetic phases as in Ref. [11]).

The magnetic-field-induced phase transitions are in some cases better visualized by plotting the real part of the susceptibility as a function of the applied field at fixed temperatures (Fig. 3).

The $H \parallel a$ data shown in the top panel of Fig. 3 reveal a change in the susceptibility slope at about 2 T, followed by a broad peak and a further tiny change in the slope in the 6–8-T region (the latter is marked by arrows) for temperatures lower than the transition temperature from the HTI to the LTI phase (the slope changes are clearly evident on the susceptibility derivative, which are shown in the

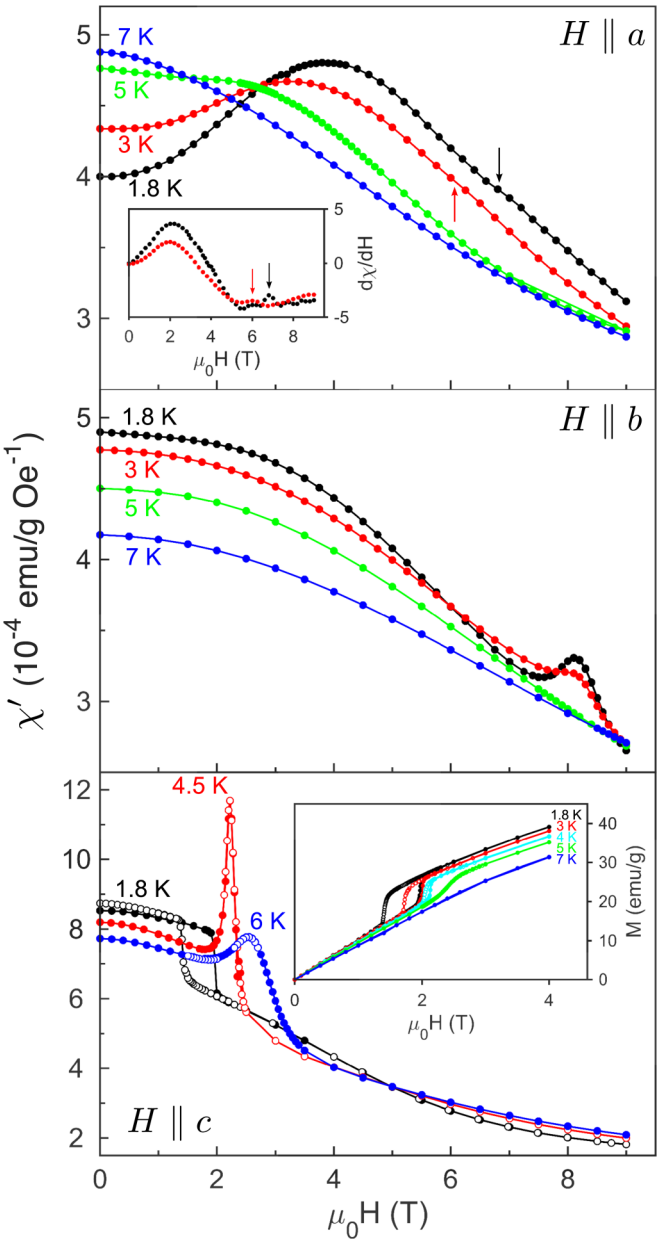

FIG. 3. Real part of the ac magnetic susceptibility at different temperatures for dc magnetic fields applied along the principle crystallographic directions. Solid (open) circles represent data measured with increasing (decreasing) field. The inset in the bottom panel shows the magnetization as a function of applied field at different temperatures.

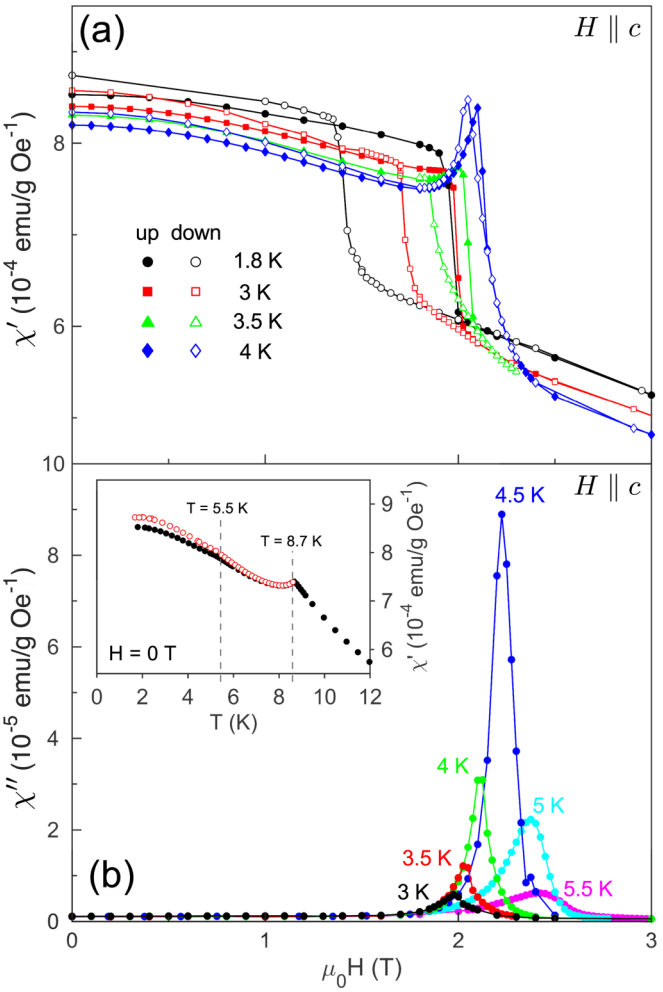

FIG. 4. (a) Magnetic field ramps clearly showing a hysteresis at the LTI-*C* transition. The extent of the hysteresis is reduced towards the HTI phase. (b) Field-dependent imaginary part of the magnetic susceptibility clearly indicating magnetic losses at the field-induced transitions. The inset shows the temperature-dependent susceptibility revealing that a field-treated sample (open symbols) behaves differently than a non-field-treated sample (solid symbols) in the temperature region corresponding to the LTI phase.

inset). The anomalous susceptibility at low temperatures suggests magnetic-field-induced modifications of the magnetic structure, which, according to the phase diagram of $Ni_3V_2O_8$ [11], should involve the LTI-HTI phase transition. We will elaborate a bit further on this when discussing the neutron diffraction results. As the HTI phase is dominated by a collinear alignment of the spine spins along the *a* axis, a magnetic field parallel to the *a* axis would induce only a spin-flop transition and a spin-flip transition at magnetic field values higher than the ones probed in this study [27]. For $H \parallel b$ (Fig. 3, bottom panel) we observe hints of field-induced phase transitions only at low temperatures (below about 3 K) and approximately 8 T. Note that for $H \parallel a$ and $H \parallel b$ no hysteresis was observed on increasing or decreasing the field, and also the imaginary component of the susceptibility (not presented) remains negligibly small upon field or temperature variations. For $H \parallel c$, a jump in the magnetization curves and a drop in the real part of the susceptibility are observed at 1.8–1.9 T (see the bottom panel of Fig. 3), signaling a field-induced transition from the LTI into the commensurate weakly ferromagnetic *C* phase, which is driven by the gain in the Zeeman energy due to the interaction with its weak ferromagnetic moment. This statement will be further justified on the basis of neutron diffraction results. Since the magnetic field is practically perpendicular to the spine spins, the observed decrease of the susceptibility could be associated with a change in the exchange stiffness after the transition to the *C* phase. The field-induced transition is hysteretic with respect to magnetic

field ramping, implying that it is of first order. With increasing temperature, the width of the hysteresis decreases, and a bump in susceptibility starts to emerge. The hysteresis disappears at about 4.5 K, and a sharp susceptibility peak appears. The divergence of the susceptibility and the absence of hysteretic behavior suggest a second-order phase transition. Note that the deduced nature of the phase transitions is in agreement with the respective symmetries of the involved magnetic structures. The LTI and the C phases possess $Cm2a1'$ and $Cm'c'a$ symmetries, respectively, which do not have a group-subgroup relationship. This is already obvious due to the different translational symmetries of the two phases, so there can be only a first-order transition between those two phases. The HTI magnetic structure has $Cmca1'$ symmetry, with $Cm2a1'$ being a subgroup of it, which therefore predicts a transition of second order. With a further increase in temperature the susceptibility peak becomes broader and finally vanishes when reaching the Néel temperature. Figure 4(a) illustrates the real component of the susceptibility in more detail, while the corresponding imaginary component is depicted in Fig. 4(b). The inset in the latter figure displays an intriguing finding, namely, that for temperatures below the HTI transition a pronounced difference in the temperature dependence of the low-field susceptibility recorded on heating from 2 K for a zero-field cooled sample and a sample exposed to fields above 2 T at 2 K exists. This behavior is in agreement with the irreversibility of the susceptibility at 1.8 K below the hysteretic-field-induced transition on up or down field ramps, which is shown in the bottom panel of Fig. 3.

The electric polarization along the crystallographic b axis P_b was measured in magnetic fields parallel to the a and c axes as a function of H at fixed T (Fig. 5, left column) and as a function of T at fixed H (Fig. 5, right column). No data are shown for $H \parallel b$ since in that case the maximum possible field is insufficient to induce the LTI $\rightarrow C$ phase transition and the LTI $\leftrightarrow$ HTI phase border is not affected much in this field range. We recall that a poling electric field $E \sim 1.3$ kV/cm was applied while cooling down the sample and was continuously applied when measuring the polarization. The top left panel of Fig. 5 depicts $P_b(H)$ for $H \parallel a$ at fixed temperatures to which the sample has been cooled in zero magnetic field. In agreement with the magnetization data, at very low temperatures (2 and 3 K) the polarization associated with the LTI phase holds up to the maximum applied field of 5 T and then is suppressed by the field only at temperatures above 4 K. This suppression is ascribed to the field-induced transition into the HTI phase, which is paraelectric. Some selected $P_b(T)$ dependencies at fixed H are plotted in the top right panel of Fig. 5. A hysteresis in both $P_b(H)$ and $P_b(T)$ is present on crossing the transitions. The bottom left panel of Fig. 5 depicts the $P_b(H)$ data for $H \parallel c$ after a zero-magnetic-field-cooling procedure. At 2 K P_b sharply falls to zero at $H_{cr} \approx 2$ T on increasing field and reappears on decreasing field at $\sim$1.5 T by sharply rising to a value which is significantly smaller than

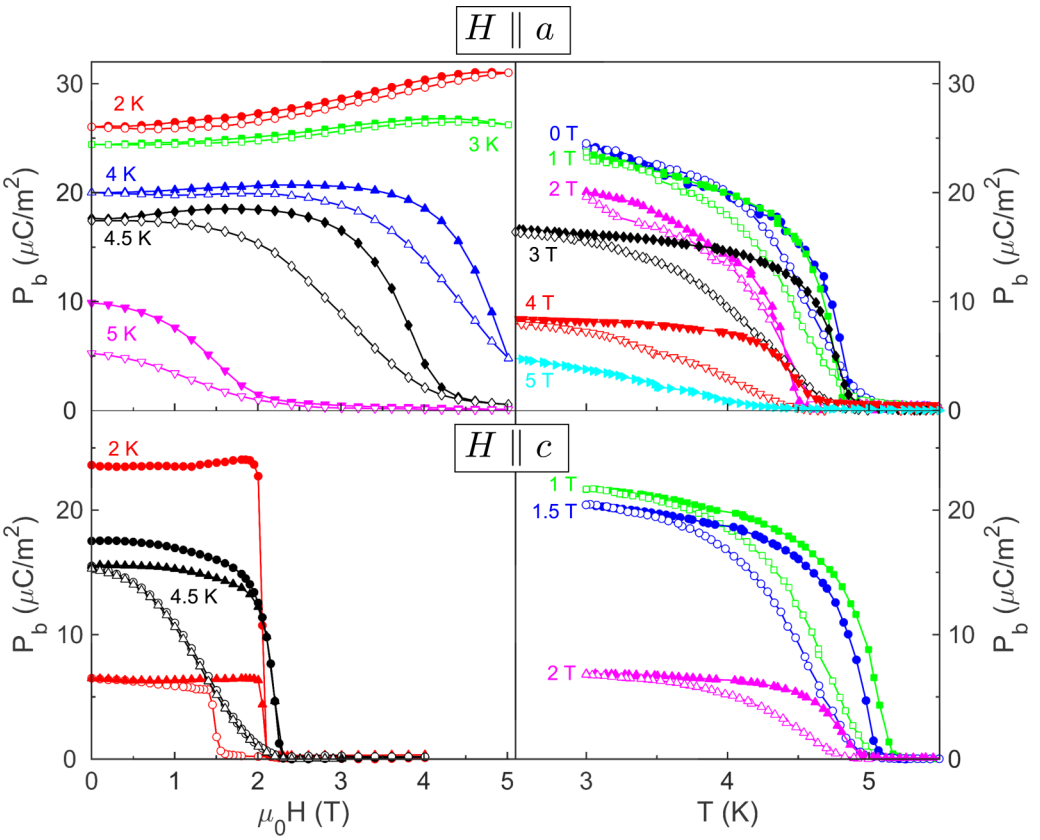

FIG. 5. Electric polarization as a function of magnetic field at fixed temperatures (left column) and as a function of temperature at fixed magnetic field (right column) with $H \parallel a$ (top row) and $H \parallel c$ (bottom row). Solid (open) symbols represent data measured with increasing (decreasing) field. In the bottom left panel circles represent a field sweep after ZFC, while triangles show data recorded after field cooling.

the one recorded after zero field cooling (ZFC). On further cycling the magnetic field the temperature hysteresis in P_b holds, and the difference between ZFC and the reentrant values of P_b remains. The disappearance of P_b above some critical magnetic field and its reappearance on reducing the field is naturally related to the field-induced transition between the polar LTI and the paraelectric C phases, already revealed in the magnetic measurements. The above-described difference in the electric polarization of the LTI phase after the ZFC procedure and after reentering it from the high-field C phase corroborates the observed differences in the magnetization, which are shown in Fig. 4(b). It is also consistent with the neutron diffraction results suggesting some differences in the LTI structure after ZFC and after reentering from the C phase, which will be discussed further below. However, the smaller LTI polarization recording on reentering could also result from the applied electric field ($\sim$1.3 kV/cm) during the magnetic field ramp not being sufficiently high to establish a single domain state. With increasing temperature both the width of the temperature hysteresis in P_b and the difference between ZFC and the reentrant values of P_b decrease (see the 4.5 K data), and the polarization, instead of rising sharply on reentering the LTI phase, reappears smoothly. At 5 K the polarization is already significantly reduced and only slowly changes with the field variation without any jump (data not shown). It finally vanishes at $T \geqslant 5.5$ K. Some selected $P_b(T)$ dependencies at fixed H along the c axis are given in the bottom right panel of Fig. 5 for fields smaller than the critical field of about 2 T. They evolve in a similar fashion and only slightly shift towards low temperatures. On approaching $H_{cr} \approx 2$ T the polarization decreases and vanishes at higher fields. We note that the observed temperature hysteresis is partly affected by the measurement conditions (a temperature sweep of 0.6 K/min was used). The critical parameters, H_{cr} and T_{cr}, determined from $P_b(H)$ and $P_b(T)$ in the above crystallographic orientations are used, along with the magnetic and neutron diffraction results, to construct the phase diagrams (Fig. 6). H_{cr} was associated with the dP/dH maximum (in absolute values), while T_{cr} was ascribed to the middle of the steepest part of $P_b(T)$ recorded on cooling and on warming. Since T_{cr} in the two cases is within the limit of the experimental error in temperature (0.2 K) we can neglect the temperature hysteresis on the LTI $\leftrightarrow$ HTI phase border.

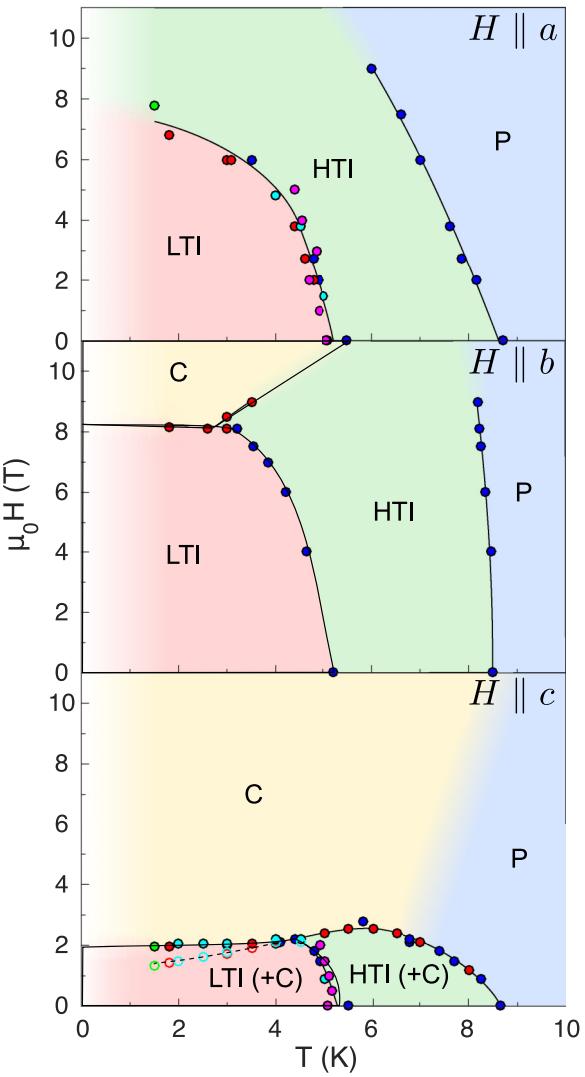

FIG. 6. Magnetic H-T phase diagrams of $(Ni_{0.9}Co_{0.1})_3V_2O_8$ for magnetic fields along the principal crystallographic axes. Red dots were obtained from the anomalies in the $\chi(H)$ curves, while the blue dots emerge from the anomalies in $\chi(T)$. Green dots represent the phase transitions observed by neutron diffraction. Light blue dots were obtained from $P_b(H)$ measurements, and magenta dots were obtained from $P_b(T)$. Open symbols denote the $C \rightarrow$ LTI phase transition in decreasing magnetic field. For $H \parallel c$ the C phase in parentheses refers to the fact that weak commensurate reflections coexist within the LTI and HTI phases after a field treatment.

B. Neutron diffraction experiments

1. $H \parallel a$

A set of 350 unique nuclear reflections according to the space group $Cmce$ has been recorded, and the results of the nuclear structure refinement agree with our previous measurements [20]. The magnetic structures have been investigated at $T = 1.5$ K for three different field values, $H = 0$, 4, and 9 T, for which more than 200 magnetic satellites have been measured. The zero-field data set corresponding to the cycloidal LTI phase could be explained by a mixture of two irreducible representations, which agrees with our previous measurements using a four-circle cryostat. Figure 7 shows the magnetic-field dependence ($T = 1.5$ K) of two magnetic satellites representative of the incommensurate cycloidal structure, while the inset depicts the evolution of a commensurate peak which is allowed in the field-induced C structure but forbidden for a ferromagnetic component due to the glide plane perpendicular to the c axis of space group $Cmce$. While the propagation vector does not change, the intensity evolution of the magnetic satellites shows two anomalies at approximately 3 and 8 T where the slope of the intensity decrease changes with increasing magnetic field (note that the intensity of the satellites does not drop to zero above 8 T). All data sets have been analyzed using the combination of the irreducible representations Γ_1 and Γ_4 (see Refs. [13,20] for more details), where all parameters from the nuclear structure refinement have been fixed while only refining the coefficients according

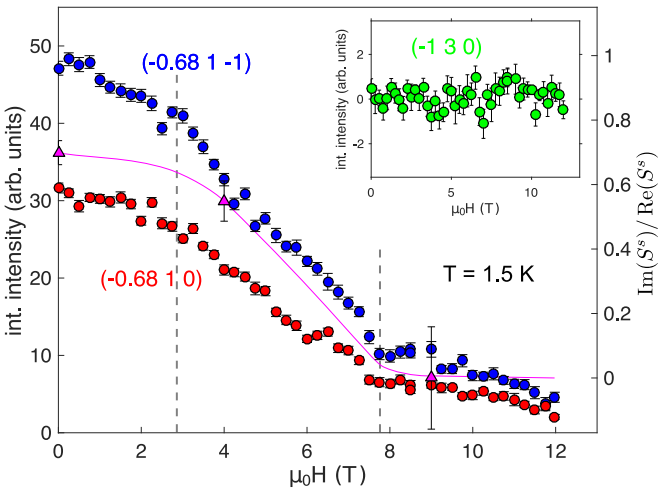

FIG. 7. Left ordinate: Integrated intensities as a function of the applied magnetic field along the a axis (solid circles). With increasing field the incommensurate reflections are weakened, while the evolution seems to reveal two kinks at 3 and 8 T. The kink at 8 T has a clear origin (i.e., the transition to the sinusoidal state accompanied by a disappearance of the b component of the spine spin), while the kink at 3 T [only clearly observable for the $(-0.68, 1, -1)$ reflection but not for $(-0.68, 1, 0)$] has no such clear physical origin. We may speculate that it reflects the onset of the cycloidal b component suppression which is already evident at 4 T (see Table I). Right ordinate: The refined ratio between the imaginary b and the real a components of the spine spins from full data collections at different field values revealing a similar evolution with magnetic field (the solid line is a guide to the eye). The inset shows the field dependence of the commensurate antiferromagnetic (130) reflection representative for the C phase.

to the symmetry-adapted basis vectors. The results in Table I suggest that the increase to $H = 4$ T reduces the magnetic moments of the spine sites, while the cycloidal envelope becomes more elliptic. As no increase of the antiferromagnetic

TABLE I. Refined components of the basis vectors for spine spins S^s given in Bohr magnetons for the magnetic structure model describing the data at $T = 1.5$ K ($\Gamma_1 + \Gamma_4$) in zero and applied field along the a axis. Note that the basis functions of Γ_1 are shifted by a phase factor of $\pi/2$ with respect to those of Γ_4. The ratio between the main and fine components of the different irreducible representations has been fixed to the value obtained in our previous zero-field analysis [20]. The main components are listed in bold.

$\mu_0 H(T)$	$S^{p,r}_{\Gamma_n}$	$x = 0.10$
0	$S^s_{\Gamma_1}$	$[-0.19(7), \mathbf{1.37(7)i}, -0.1(2)]$
	$S^s_{\Gamma_4}$	$[\mathbf{1.96(3)}, 0.121(2)i, -0.013(1)]$
	χ^2 (R_F)	9.2 (14.3)
4	$S^s_{\Gamma_1}$	$[-0.24(8), \mathbf{0.9(1)i}, 0.0(2)]$
	$S^s_{\Gamma_4}$	$[\mathbf{1.64(4)}, 0.101(3)i, -0.017(1)]$
	χ^2 (R_F)	11.3 (14.3)
9	$S^s_{\Gamma_1}$	$[-0.2(2), \mathbf{0.0(2)i}, 0.0(1)]$
	$S^s_{\Gamma_4}$	$[\mathbf{1.26(4)}, 0.078(2)i, -0.022(1)]$
	χ^2 (R_F)	4.7 (21.2)

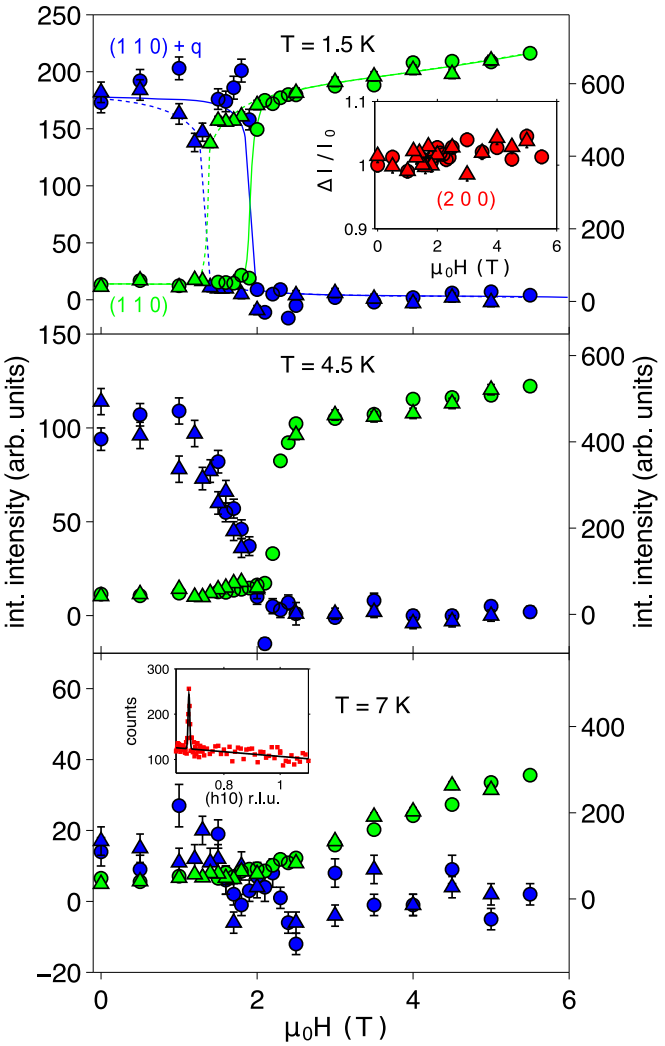

FIG. 8. Integrated intensities of incommensurate (blue symbols, left ordinate) and commensurate (green symbols, right ordinate) magnetic reflections as a function of the applied magnetic field along the c axis. Data recorded with increasing ($\mathbf{q} = \mathbf{q}_0$) and decreasing ($\mathbf{q} = \mathbf{q}_H$) field are represented by circles and triangles, respectively. In the top panel the solid and dashed lines are guides to the eye, while the inset shows the field evolution of a nuclear reflection. The data show a clear hysteretic behavior at $T = 1.5$ K, which is reduced for $T = 4.5$ K and absent for $T = 7$ K. The inset in the bottom panel shows a q scan along the a^* direction before the first application of the external field, clearly illustrating the absence of the (110) reflection.

$(-1\ 3\ 0)$ and no additional intensity on the nuclear structure peaks were observed, it seems that the magnetic moments are entirely modulated according to $\mathbf{q} = (0.32\ 0\ 0)$. We cannot rule out the formation of new magnetic satellites, which is, however, very unlikely. Interestingly, at $H = 9$ T, above the high-field change of the susceptibility slope visible in Fig. 3 (top panel), the envelope of the cycloidally modulated spine spins is effectively flattened towards the a axis, while the cross-tie spins remain unaffected by the applied field within the experimental precision [25]. The high-field magnetic structure at $T = 1.5$ K is therefore topologically equivalent to the HTI structure. The ratio between the refined real a axis and the imaginary b axis components of the spine spins is plotted in

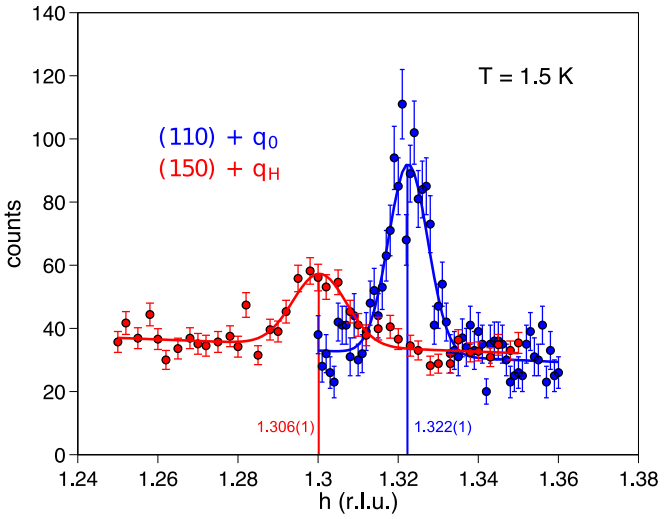

FIG. 9. The q scans along the a^* direction across the (110)+$\mathbf{q}_0$ and (150)+$\mathbf{q}_H$ magnetic satellites at $H = 0$ T before and after applying a magnetic field along the c axis. The shift in the position clearly shows a smaller incommensurability for the field-treated state.

Fig. 7, which coincides with the shown field evolution of the magnetic Bragg reflection intensities. Regarding the feature at 2.5–3 T which is clearly present only for the $(-0.68\ 1\ -1)$ reflection and not for $(-0.68\ 1\ 0)$, we suggest that it reflects specific features in the field evolution of the cycloid. In particular, it is close to the maximum observed in χ vs $H \parallel a$ dependence (Fig. 3), which could be related to a precursor of the further significant suppression of the b component of the cycloid observed at 4 T (Table I).

2. $H \parallel c$

In order to verify the nuclear and magnetic structures at zero field and $T = 1.5$ K 40 and 60 reflections were measured, respectively. According to the pronounced hysteresis observed in the magnetic susceptibility for the LTI $\rightarrow$ C transition, three different Bragg reflections were measured as a function of magnetic field at three different temperatures. In Fig. 8 it can be seen that the intensity of the incommensurate magnetic peak (1.32 1 0) from the cycloidal structure vanishes at the phase transition into the commensurate C phase where the (1 1 0) reflection emerges. In agreement with the macroscopic data a clear hysteresis in the field-dependent evolution of the magnetic intensities can be observed when the field is ramped up and down. Furthermore, the propagation vector changes from $\mathbf{q}_0 = (0.322\ 0\ 0)$ to $\mathbf{q}_H = (0.306\ 0\ 0)$, where $\mathbf{q}_0$ refers to a zero-field-cooled sample and $\mathbf{q}_H$ denotes the propagation vector of the reentrant phase after ramping the field across the LTI $\rightarrow$ HTI phase transition (see Fig. 9) [26]. In analogy to the susceptibility the hysteresis becomes less pronounced when approaching the zero-field phase-transition temperature into the HTI phase. Note that the data shown here were taken after previous field ramps and that the (110) reflection, corresponding to the C phase, reveals nonzero intensity after ramping the field down to zero. Therefore, this suggests the coexistence of the LTI/C and HTI/C phases in the respective temperature ranges. The absence of the (110) reflection before the very first application of magnetic field along the c axis is shown in the inset of the bottom panel. Due to the lack of a full data set of C-type reflections at $H = 0$ T we can only estimate that at $T = 1.5$ K the magnetic moments on both sites are roughly 10 times smaller in comparison to the values obtained at $H = 3$ T. The inset in the upper panel of Fig. 8 depicts the field dependence of a nuclear reflection which does not show a clear increase in intensity. Furthermore, the refinement of a nuclear data set at $T = 1.5$ K and $H = 3$ T did not reveal a significant field-induced ferromagnetic component along the c

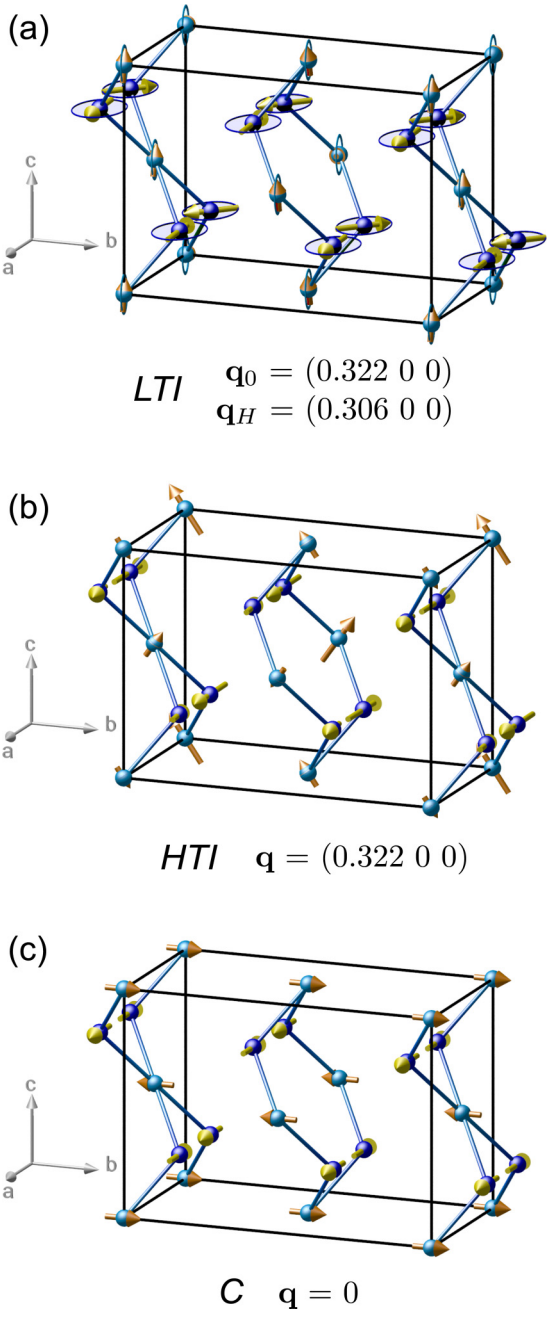

FIG. 10. Visualization of the magnetic structures of the (a) cycloidally modulated LTI phase, (b) the sinusoidally modulated HTI, and the (c) commensurate C phase. Note that the cross-tie spins (orange) are overscaled by a factor of 5 with respect to the spine spins (yellow) in (a) and (b).

axis. Note that in the parent compound $Ni_3V_2O_8$ no significant c spin component could be observed up to 8 T [13]. From the magnetization jump at the LTI $\rightarrow$ C transition shown in the inset of the bottom panel of Fig. 3 we can see that the induced ferromagnetic moment along the c axis is smaller than $0.2\mu_B$ per magnetic ion, which is beyond the limit of detectability given the fact that the additional magnetic intensity in an unpolarized neutron diffraction experiment is found superposed on the strong nuclear reflections. Particularly for the (200) reflection, the magnetic structure factor with an induced magnetic moment of $0.2\mu_B$ would be 50 times smaller than the nuclear structure factor, yielding $I/I_0 = 1.0004$. A set of 50 commensurate magnetic Bragg reflections was recorded at $T = 1.5$ K with an applied magnetic field of 3 T, which is within the field-induced C phase. The magnetic intensities could be explained by a single irreducible representation with a collinear alignment of the spine spins along the a axis, which in turn polarizes the cross-tie spins along the b axis, i.e., the direction imposed by symmetry restrictions.

The magnetic structure at zero field was investigated before ($\mathbf{q}_0$) and after the field ($\mathbf{q}_H$) was ramped up to 6 T. No significant change could be observed on the spine spins; however, the cross-tie spins showed a significant increase of the b-axis component. Before the application of the magnetic field, the refined cross-tie moment is $[-0.1(1)i\ -0.03(9)\ 0.20(8)]$ ($R_F = 10.8$), in agreement with our previously published data [20], while it becomes $[0.0(1)i\ -0.4(1)\ 0.20(9)]$ ($R_F = 13.2$) in the reentrant phase. This agrees with the observation of an increased response in the susceptibility of a field-treated sample for $H \parallel c$ seen in Fig. 4. One could suppose that such differences in the ordered magnetic moments could be related to a partially disordered or short-range ordered component; however, our analysis of the peak shape did not allow us to make any confident statement because of the rather weak intensities and insufficient statistics for this kind of analysis. A further set of commensurate peaks was measured at 7 and 5.5 T which still could be explained by the commensurate antiferromagnetic structure. This fact agrees with the bottom panel of Fig. 8, which shows that the intensity of the commensurate antiferromagnetic Bragg peak (1 1 0) constantly increases above 2 T. As pointed out before, (h k 0) reflections with h and k being odd are absent due to the glide plane perpendicular to the c axis. Therefore, an induced ferromagnetic moment within the paramagnetic phase can be ruled out below 7 K.

IV. CONCLUSION

All susceptibility and electric polarization curves shown in Sec. III A and the information from the neutron diffraction experiments (Sec. III B) were used to draw the magnetic H-T phase diagrams along the three main crystallographic axes (Fig. 6). As already reported earlier [20], the main differences in comparison to the undoped compound are, on the one hand, the stabilization of the multiferroic cycloidal phase LTI down to at least 1.8 K and, on the other hand, lower respective transition temperatures at zero magnetic field. Our previous results together with the theoretical work presented in Ref. [13] allowed us to draw detailed conclusions concerning the fine balance between the single-ion anisotropy and the competing exchange interactions. We recall that the increased q_x component of the propagation vector and the larger temperature stability range of the HTI phase suggested an increased single-ion anisotropy K due to Co doping which is compensated by larger J_2/J_1 and K/J_1 ratios (J_1 and J_2 denote the exchange coupling constants between nearest and next-nearest neighbors along the spine spin chain, respectively). While the magnetic phase diagram for a magnetic field along the hard axis b is very similar for the commonly involved phases, the LTI and HTI phases show a stronger instability in $(Ni_{0.9}Co_{0.1})_3V_2O_8$ for applied fields along the a and c directions because for a given temperature significantly lower magnetic fields are necessary to induce the respective transitions. This is most pronounced for the HTI phase with $H \parallel c$, which in the doped compound exists only below 2.5 T, while in the parent compound the stability range extends to 6 T. Within the HTI phase the dominant energy term is the single-ion anisotropy which favors a collinear spin alignment at the cost of exchange energy (which only becomes more important at lower temperatures) as the ordered value of the magnetic moment is reduced because of the sinusoidal modulation. Due to the larger single-ion anisotropy a smaller external magnetic field is therefore sufficient in order to induce the C phase. In addition, we observed a smaller q_x component of the propagation vector in the reentrant phase. As the competing interactions along the spine chains determine the incommensurate propagation vector of the magnetic structures according to $\cos[(1 - q_x)\pi] \approx -J_1/4J_2$, a smaller q_x value would therefore indicate a reinforcement of the nearest-neighbor interaction J_1 with respect to the next-nearest-neighbor interaction J_2. This observation is well in line with the remanent features of the C phase, which consists of collinear alignments of cross-tie and spine spins. For magnetic fields applied to the a axis two anomalies are observable in the field dependence of the integrated magnetic reflections (Fig. 7). While the anomaly at 7.8 T is clearly related to the field-induced LTI $\rightarrow$ HTI transition, the change in slope visible for $(-0.68\ 1\ -1)$ is not entirely clear. Due to the limited number of complete neutron diffraction data sets it can only be speculated that the cycloidal envelope starts to shrink and become more elliptic for magnetic fields stronger than a critical value, which also roughly corresponds to the maximum of the field-induced susceptibility for $H \parallel a$ (see Fig. 3). Furthermore, our findings reveal a rather unusual phase boundary between the C and paramagnetic phases for $H \parallel c$, where the application of a magnetic field drives the disordered phase into an antiferromagnetically ordered one, the so-called induced antiferromagnetism, at least for temperatures close to T_N. Our neutron diffraction results undoubtedly prove the stability of the C phase up to 7 K (see Fig. 8, bottom panel). The most interesting result concerns the hysteresis at the phase transition between the LTI and C phases for $H \parallel c$ which is observable in the susceptibility, in the polarization, and in the neutron diffraction data and disappears for temperatures approaching the HTI phase. Hysteretic behavior has been reported for other multiferroic compounds [28,29], such as $TbMnO_3$ and $DyMnO_3$; however, either an incommensurate-to-commensurate lock-in of the propagation vector with a small change in $\mathbf{q}$ [30,31] or a continuous incommensurate-to-incommensurate transition with a change of modulation

[32] is concerned, respectively, where the electric polarization flop occurs. In $(Ni_{0.9}Co_{0.1})_3V_2O_8$ the case is different as the high-field phase is a $\mathbf{q} = 0$ antiferromagnet, which means that the modulation drastically changes. All our employed methods furthermore suggest a different magnetic structure upon reentering the low-field phase, which is undoubtedly manifested in the higher magnetization response, in the lower polarization, and in the change in the propagation vector. Furthermore, we have observed the coexistence of incommensurate reflections within the LTI and HTI phases and weak commensurate ones originating from the *C* magnetic structure after the sample has been driven across the respective transitions on increasing and then decreasing field. We can estimate that the scattering at those commensurate positions stems from magnetic moment values of roughly a tenth compared to those at $H = 3$ T well within the *C* phase. The propagation vector in the parent compound $Ni_3V_2O_8$ is sensitive to the temperature throughout the LTI phase, and our results show the sensitivity to a magnetic field treatment, which raises a question about a continuum or manyfold of ground and metastable states within the LTI phase, not only in this material but in multiferroics in general, as the magnetic structure at certain conditions seems to be dependent on the path on which the system is driven towards those conditions [33]. Our data presented here show a significantly increased cross-tie moment in the reentrant phase. Given the fact that the *C* structure is commensurate with a collinear cross-tie spin alignment along the *b* axis [see Fig. 10(c)], an increased *b* component and a smaller propagation vector (i.e., a longer-pitched magnetic periodicity towards commensurability) in the reentrant phase are arguments for remanent features of the *C* structure. In other words, when the systems is driven from the weak ferromagnetic and single-domain *C* phase ($\mathbf{k} = 0$), established in high fields, to the incommensurate zero-field phase, it tends to rest in a local (metastable) energy minimum state with a wave vector closer to $\mathbf{k} = 0$. The latter could differ from the incommensurate state which is stabilized after a zero-field-cooled thermodynamic path. An increasing J_1/J_2 ratio, remanent features of the *C* phase within the incommensurate magnetic structures, and the existence of commensurate magnetic peaks after crossing the phase boundaries on decreasing fields to $H = 0$ T corroborate our conclusions. A possible origin for such local minima on reentering from the high-field state could be magnetic and structural inhomogeneities inherent in doped crystals.

ACKNOWLEDGMENTS

This work was partially supported by the Russian Scientific Foundation (Project No. 16-12-10531). The work carried out in Minsk was supported in part by BRFFI-RFFI Grants No. F14R-094 and No. F16R-139. We acknowledge the financial support from the Spanish Ministry of Economy and Competitiveness, through the MAT2014-56063-C2-1-R and MAT2015-71664-R projects, and funding from the European Union's FEDER (Spain) program.

[1] M. Fiebig, J. Phys. D **38**, R123 (2005).
[2] D. I. Khomskii, J. Magn. Magn. Mater. **306**, 1 (2006).
[3] W. Eerenstein, N. D. Mathur, and J. F. Scott, Nature (London) **442**, 759 (2006).
[4] S.-W. Cheong and M. Mostovoy, Nat. Mater. **6**, 13 (2007).
[5] R. Ramesh and N. A. Spaldin, Nat. Mater. **6**, 21 (2007).
[6] T. Kimura, Y. Sekio, H. Nakamura, T. Siegrist, and A. P. Ramirez, Nat. Mater. **7**, 291 (2008).
[7] Z. Wang, N. Qureshi, S. Yasin, A. Mukhin, E. Ressouche, S. Zherlitsyn, Y. Skourski, J. Geshev, V. Ivanov, M. Gospodinov *et al.*, Nat. Commun. **7**, 10295 (2016).
[8] H. Fuess, E. F. Bertaut, R. Pauthenet, and A. Durif, Acta Crystallogr., Sect. B **26**, 2036 (1970).
[9] E. E. Sauerbrei, R. Faggiani, and C. Calvo, Acta Crystallogr., Sect. B **29**, 2304 (1973).
[10] N. Rogado, G. Lawes, D. A. Huse, A. P. Ramirez, and R. J. Cava, Solid State Commun. **124**, 229 (2002).
[11] G. Lawes, M. Kenzelmann, N. Rogado, K. H. Kim, G. A. Jorge, R. Cava, A. A. Aharony, O. Entin-Wohlmann, A. B. Harris, T. Yildirim *et al.*, Phys. Rev. Lett. **93**, 247201 (2004).
[12] G. Lawes, A. B. Harris, T. Kimura, N. Rogado, R. J. Cava, A. Aharony, O. Entin-Wohlman, T. Yildirim, M. Kenzelmann, C. Broholm *et al.*, Phys. Rev. Lett. **95**, 087205 (2005).
[13] M. Kenzelmann, A. B. Harris, A. Aharony, O. Entin-Wohlman, T. Yildirim, Q. Huang, S. Park, G. Lawes, C. Broholm, N. Rogado *et al.*, Phys. Rev. B **74**, 014429 (2006).
[14] G. Ehlers, A. A. Podlesnyak, S. E. Hahn, R. S. Fishman, O. Zaharko, M. Frontzek, M. Kenzelmann, A. V. Pushkarev, S. V. Shiryaev, and S. Barilo, Phys. Rev. B **87**, 214418 (2013).
[15] H. Szymczak, M. Baran, R. Szymczak., S. N. Barilo., G. L. Bychkov, and S. V. Shiryaev, Acta Phys. Polonica A **111**, 71 (2007).
[16] J. Zhao, Q. Huang, C. de la Cruz, S. Li, J. W. Lynn, Y. Chen, M. A. Green, G. F. Chen, G. Li, Z. Li *et al.*, Nat. Mater. **7**, 953 (2008).
[17] A. A. Mukhin, V. Y. Ivanov, A. M. Kuz'menko, A. S. Prokhorov, A. A. Pronin, S. N. Barilo, G. L. Bychkov, and S. V. Shiryaev, JETP Lett. **91**, 147 (2010).
[18] Q. Zhang, W. Knafo, P. Adelmann, P. Schweiss, K. Grube, N. Qureshi, T. Wolf, H. v. Löhneysen, and C. Meingast, Phys. Rev. B **84**, 184429 (2011).
[19] A. Kumarasiri and G. Lawes, Phys. Rev. B **84**, 064447 (2011).
[20] N. Qureshi, E. Ressouche, A. A. Mukhin, V. Y. Ivanov, S. N. Barilo, S. V. Shiryaev, and V. Skumryev, Phys. Rev. B **88**, 174412 (2013).
[21] N. Qureshi, H. Fuess, H. Ehrenberg, T. C. Hansen, C. Ritter, K. Prokes, A. Podlesnyak, and D. Schwabe, Phys. Rev. B **74**, 212407 (2006).
[22] N. Qureshi, H. Fuess, H. Ehrenberg, T. C. Hansen, C. Ritter, P. Adelmann, C. Meingast, T. Wolf, Q. Zhang, and W. Knafo, J. Phys. Condens. Matter **20**, 095219 (2008).
[23] N. Qureshi, H. Fuess, H. Ehrenberg, T. C. Hansen, C. Ritter, T. Wolf, C. Meingast, Q. Zhang, W. Knafo, and H. von Löhneysen, J. Phys. Condens. Matter **20**, 235228 (2008).
[24] J. C. Matthewman, P. Thompson, and P. J. Brown, J. Appl. Crystallogr. **15**, 167 (1982).
[25] We want to point out that the cross-tie spin moment was found to be larger even at $H = 0$ T in the experiment with $H \parallel a$

in comparison to our previous experiment using a four-circle cryostat and to our results shown in Sec. III B 2. Therefore, we limit ourselves to a qualitative discussion of the cross-tie moments with fields along the *a* axis.

[26] Note that we have measured the *q* scan across the (110) reflection only before applying a magnetic field and that we have measured the *q* scan across the (150) reflection only after the field has been ramped down. Even though we have not done *q* scans on the same reflection, the two presented scans in Fig. 9 prove the shift in the propagation vector.

[27] J. Wang, M. Tokunaga, Z. Z. He, J. I. Yamaura, A. Matsuo, and K. Kindo, Phys. Rev. B. **84**, 220407(R) (2011).

[28] T. Kimura, T. Goto, H. Shintani, K. Ishizaka, T. Arima, and Y. Tokura, Nature (London) **426**, 55 (2003).

[29] O. Prokhnenko, R. Feyerherm, E. Dudzik, S. Landsgesell, N. Aliouane, L. C. Chapon, and D. N. Argyriou, Phys. Rev. Lett. **98**, 057206 (2007).

[30] N. Aliouane, D. N. Argyriou, J. Strempfer, I. Zegkinoglou, S. Landsgesell, and M. v. Zimmermann, Phys. Rev. B **73**, 020102(R) (2006).

[31] N. Aliouane, K. Schmalzl, D. Senff, A. Maljuk, K. Prokes, M. Braden, and D. N. Argyriou, Phys. Rev. Lett. **102**, 207205 (2009).

[32] J. Strempfer, B. Bohnenbuck, M. Mostovoy, N. Aliouane, D. N. Argyriou, F. Schrettle, J. Hemberger, A. Krimmel, and M. v. Zimmermann, Phys. Rev. B **75**, 212402 (2007).

[33] It is worth noting that our very recent unpublished results on Co-doped $MnWO_4$, acquired when the current paper was under review, also reveal a well-pronounced irreversibility of the zero-field state obtained after zero field cooling and after reentering from the corresponding magnetic field-induced phase. The irreversibility is manifested in both the electric polarization and bulk magnetization as well as in the propagation vector.